LAWRENCE
LIVERMORE
NATIONAL
LABORATORY

UCRL-JRNL-214764

Investigation of near infrared autofluorescence imaging for the detection of breast cancer

S. G. Demos, R. Bold, R. deVere White, R. Ramsamooj

August 23, 2005

Journal of Selected Topics in Quantum Electronics

Investigation of near infrared autofluorescence imaging for the detection of breast cancer

Stavros G. Demos[a,b], Richard Bold[b], Ralph deVere White[b], Rajen Ramsamooj[b],

[a] Lawrence Livermore National Laboratory, Livermore, CA 94551

[b] UC Davis Medical School, Medical Center, Sacramento, CA 95817

Abstract

Detection of breast cancer in fresh tissue obtained from surgery is investigated using Near-infrared autofluorescence imaging under laser excitation at 532-nm and 632.8-nm. The differences in intensity between the three main components of breast tissue (cancer, fibrous and adipose) are estimated and compared to those obtained from cross-polarized light scattering images recorded under polarized illumination at 700-nm. The optical spectroscopic images for each tissue sample were subsequently compared with the histopathology slides. The experimental results indicate that the intensity of the near-infrared emission is considerably different in breast cancer compared to that of the adjacent non-neoplastic tissues (adipose and fibrous tissue). The experimental results suggest that 632.8-nm excitation offers key advantages compared to 532-nm excitation.

Introduction

Breast cancer remains a major health problem. Despite the development of mammography and the implementation of regular screening programs, it is estimated that approximately one third of women with breast cancer in the US will present with disease that is readily apparent on physical examination. Although the mammographic and ultrasound criteria for malignancy are well validated, there still remains a large fraction of lesions with indeterminate preoperative imaging that mandate histologic evaluation to exclude malignancy. With the increasing use of hormonal replacement therapy in postmenopausal women, the density of the breast tissue increases. This increase in tissue density is expected to limit the ability of mammography to be effective in the early detection of breast cancer [1, 2] and lead to an increase in the number of excisional biopsies performed for diagnostic purposes. The histologic examination is currently performed by selecting one of the well-developed invasive breast biopsy techniques (excisional biopsy, axillary node dissection, sentinel node dissection, and fine needle aspiration) depending on the location, size, palpability, and characteristics of the abnormality.

As breast excisions remain one of the most common surgical operations in the United States, segmental mastectomy or “lumpectomy” is performed for both the diagnosis of breast cancer as well as the treatment [3]. In the current setting, immediate histologic analysis is not possible or even practical. While frozen section analysis is available, there are technical limitations to cutting certain types of tissue (eg. adipose tissue). Therefore, it is essential that new tools be developed to replace or complement existing technology. Technology that can offer detection and delineation of tumor margins in real time may be very useful to a surgeon during a diagnostic or therapeutic procedure.

Photonic technology is currently playing an important role in the development of new medical diagnostic tools. Stimulated by advances in the modeling of light propagation in tissues, “Optical Mammography” [4-8] (a system that will be able to image breast tumors using near

infrared light) has evolved to become a promising imaging tool. Using optical spectroscopy methods, also referred to as “optical biopsy” methods, various research groups have demonstrated high sensitivity for cancer detection in various parts of the body [9]. The presence of cancer specific optical “signatures” is necessary in order to devise optical methods for cancer detection. These optical “signatures” may arise from differences in the biochemical and/or structural characteristics of the tissues. Although there has been a relatively smaller effort in utilizing the optical biopsy approaches to detect breast cancer, recent studies have indicated that breast tissue components can be differentiated using Raman spectroscopy [10-12] and light scattering spectroscopy [13,14]. The drawback of Raman scattering methods in tissues is that the signal is weak and it is usually accompanied by an intense background giving rise to problems regarding data acquisition, signal processing and accuracy. Zhang, et al. have investigated the spectral, polarization and temporal characteristics of the far-red and near-infrared (NIR) emission beyond 650 nm from breast human and chicken tissue samples under low intensity laser excitation at 532 and 633 nm. The lifetime of this emission was found to be on the order of 1 ns. The differences in intensity of the far-red emission spectral wing were utilized to image adipose and breast components in the chicken tissue model [15]. It was also suggested (using tissue samples that were separated into large homogeneous parts of normal and tumor tissue) that the NIR autofluorescence intensity from human breast cancer is different to that from normal tissue and potentially could be used to detect breast cancer. More recent studies using fresh tissue specimens containing normal and cancer tissue from various body organs have indicated the potential of NIR autofluorescence imaging under long wavelength excitation for cancer detection [16, 17]. It was hypothetized that porphyrins may be the fluorophore giving rise to changes in the NIR autofluorescence intensity in cancer tissue [16]. This change may be the result of a change in the production of porphyrins in neoplasia due to change in the heme-biosynthetic pathway. The utilization of NIR autofluorescence imaging in combination with cross-polarized light scattering imaging in the NIR spectrum demonstrated

promising results for the detection of cancer and delineation of tumor margins in the bladder [17].

The objective of this study is to determine using fresh surgical specimens the potential of the near-infrared autofluorescence method under long-wavelength excitation for real time detection and imaging of breast cancer lesions in a clinicaly relevant setting. We have focused our attention in determining the relative intensity arising from the main human breast tissue components (tumor, adipose and fibrous tissues). We have also evaluated the excitation wavelength that offers the best results as well as the improvement in contrast compared to that obtained by light scattering alone.

Experimental setup

The spectroscopic imaging experiments were carried out using a compact experimental system located at the UC Davis Medical Center Hospital in Sacramento, CA. This system has been described in detail elsewhere [16]. Breast cancer specimens from patients undergoing surgical resection were accrued under an approved IRB protocol. The specimens were collected in a prospective fashion with prior consent from the patients. Prior to fixation in formalin, breast cancer specimens were examined by the pathologist and a representative segment (~ 3.0 x 3.0 x 0.4 cm) of the tumor with surrounding normal breast parenchyma was procured for spectroscopic examination. Each sample was positioned between two parallel glass slides on a sample holder and slightly compressed. The images of the specimens were acquired within 30 minutes after surgery using a liquid nitrogen cooled CCD detector coupled to a camera lens. A 700-nm Long-Pass (LP) filter was positioned in front of the camera lens. This filter in combination with the response spectrum of the CCD imaging camera determined the spectral range of the emitted light by the tissue (700-1000-nm) that was selected for image acquisition.

The photoexcitation used to acquire the autofluorescence images of the specimens was provided by a 632.8-nm He-Ne laser and by a 532-nm diode-pumped laser. The laser light was transmitted to the imaging compartment of the system using optical fibers. The center portion of the diverging output beams from each fiber were used to provide nearly uniform illumination of the sample. A narrow band interference filter was positioned in front of the output of each fiber to ensure monochromatic illumination. The spatial map of each illumination beam was obtained by capturing the emission image of a fluorescing card and used to normalize the intensity of the images of the tissue specimens (via pixel by pixel division of the two images). The spectral range used to record the autofluorescence images of the tissues was the same for both, 532-nm and 632.8-nm excitation. The power flux on the sample was on the order of 0.5 mW/cm^2 for both excitation wavelengths.

The cross-polarized light scattering images of the samples were recorded using a first polarizer positioned in front of the camera lens with its polarization orientation orthogonal to that of a second polarizer positioned at the output of a fiber bundle that delivers the illumination from a white light source. The wavelength selection was achieved using a 40-nm bandwidth interference filter centered at 700-nm that was positioned at the output of illumination fiber bundle.

The samples submitted for spectroscopic examination were then formalin fixed, paraffin embedded, sectioned and stained with hematoxylin and eosin using standard techniques. These spectroscopic images were subsequently compared with the histopathology map of the sampled tissue. Typically, there were small differences in the outline of the images of the H&E stained sections and that of the corresponding optical images. This difference was due to the fact that during the optical imaging experiments the specimens were held between glass slides vertically while upon completion of measurements, they were positioned in small cassettes for further processing. The position of these specimens in the cassette (which determined their

outline in the H&E stains) was not exactly the same as during the optical imaging measurements, especially for the larger specimens or those containing soft adipose tissue. A pathologist viewed the hematoxylin & eosin (H&E) stained paraffin section of each specimen by light microscopy and prepared an outline of the cancer and non-cancerous areas for direct comparison to the captured optical images. The difference in intensity in the optical images between the tissue components (discussed below) allowed for their identification and correlation to the histopathology map of the specimen as revealed by the H&E stain.

Experimental results

Thirty specimens from twenty-two different patients were examined. Seven were excluded due to interference from dyes used during the surgical procedure or inking of margins. Another five were also excluded because they contained only tumor or only normal tissue. The experimental results from the 18 remaining tumors from 16 different patients included in this study yielded significant differences in the relative intensity between tumors and the normal tissue as recorded in the NIR autofluorescence images under excitation with both, 532-nm and 632.8-nm excitation.

Figures 1 and 2 show representative examples of our experimental results. Figure 1 shows the NIR autofluorescence image under 532-nm excitation (a), and 632,8-nm excitation (b) from a ≈ 3-cm X 3-cm human breast tissue, ≈6-mm thick. A contrast-enhanced hematoxylin & eosin (H&E) stained paraffin section of the same specimen is shown in figure 1c. In the later image, the darker in intensity feature (indicated by an arrow) represents the cancerous section of the specimen. The surrounding tissue is mostly normal fatty tissue. Figure 1d shows the intensity profile of the image along a vertical line passing through the middle of the tumor. The green and red line profiles correspond to the intensity of the NIR autofluorescence image under 532-nm and 632.8-nm excitation, respectively. Comparison of the H&E stain histopathology map (figure

1c) to the spectroscopic images (shown in figures 1a and 1b and the image intensity profile in figure 1d) demonstrates that the area of enhanced emission corresponds to the location of the tumor. In addition, the margins of the tumor are also visible.

Figure 2 shows another example from a ≈ 2.8x4 cm^2, 0.5 cm thick section of breast tissue that was also obtained from surgery. The images are arranged in the same order as described above for figure 1. This figure also demonstrates the correlation of the area of enhanced emission in the NIR autofluorescence images to the location of the tumor as seen in the H&E stain section. The tissue surrounding the tumor (which is the darker in intensity feature in the image of the H&E stain) is mostly normal fatty tissue. The correlation between the histological findings and the optical imaging examination as described above has been very consistent. In all cases, the tumor tissues exhibited optical characteristics similar to those illustrated in figures 1 and 2. However, the relative intensities between normal and cancer tissue components were somewhat different among specimens from different patients. In addition, we found that the autofluorescence intensity was different between normal fibrous tissue and adipose tissue, the two main components of human breast. Consequently, a statistical analysis to compare the intensity from breast tumors to normal breast tissue requires separate analysis of tumor intensity to each of the normal tissue components.

From the 18 specimens used in this study, all but one contained tumor tissue and normal adipose tissue. It was therefore straightforward to extract the statistical behavior of the NIR autofluorescence intensity from tumors and compare it against that of the normal adipose tissue. In addition, 7 specimens contained all main tissue components including tumor, fibrous tissue and adipose tissue. From these specimens we were able to also obtain statistical results regarding the difference in intensity between malignant tumors and fibrous tissue and between fibrous and adipose tissue.

From the NIR autofluoresccence and cross-polarized light scattering images from the 18 specimens used in the pilot study, we calculated the intensity ratio between the main breast tissue components by dividing the average intensity in the tumor area of the image over that in the normal adipose tissue and fibrous tissue. The average image intensity (and standard deviation) from each tissue component was obtained using commercially available software (WinView/32, Roper Scientific, Inc., Tucson, AZ). As guidance for the location of each tissue component we used the H&E stain map of the same specimen. Depending on the size of each tissue component, the area (number of pixels) of the image used for averaging was different. In particular, we avoided borderline regions between tissue components where image intensity can be interfered by the signal in the adjacent tissue components. As indicated in the intensity profile shown in figure 1d, the width of this borderline region is smaller than 1 mm. For small lesions having diameter on the order of 1 mm, statistics was acquired from the central region of the lesion's image.

The ratio of the experimentally measured intensities between cancer , fibrous, and adipose tissue components under both, 532-nm and 632.8-nm excitation is illustrated in figure 3a, 3b and 3c. These results are complemented by the corresponding intensity ratios obtained from the cross-polarized light scattering images at 700-nm. More specifically, figure 3a shows the intensity ratio between cancer and adipose tissue from the 17 specimens containing both components under 632.8 nm excitation (solid circles), 532-nm excitation (solid squares), and under 700-nm illumination (x). The analogous intensity ratios between cancer over fibrous tissue and fibrous over adipose tissue are shown in figures 3b and 3c, respectively. The experimental results demonstrate that the ratio between cancer and normal tissue in all NIR autofluorescence images was higher than 1, indicating that the tumor intensity was higher than that of the normal tissue. The mean values of the intensity ratios from all experimental results and their standard deviations are summarized in table 1.

The images of the specimens shown in this manuscript in figures 1, 2 and 4 are from cases 17, 9, and 10, respectively. The results from the 18 specimen shown in figure 3 were originating from 16 patients. More specifically, specimens 6 and 7 are from the same patient as well as specimens 14 and 15. Most of the patients were diagnosed with ductal carcinoma (13 patients in total) while 3 (cases 3, 14&15 and 18) with lobular carcinoma,

The ability of NIR autofluorescence imaging to detect cancer may be useful in a clinical setting in situations where visual examination of the tissue may be inconclusive. This is demonstrated in the example shown in figure 4 where images of a tissue specimen that contains tumor, adipose and fibrous tissue are shown. More specifically, the NIR autofluorescence images of this specimen under 532-nm and 632.8-nm excitation are shown in figure 4a and 4b, respectively, while figure 4c shows a color photograph of the same specimen. Figure 4d shows the H&E stain of this specimen. The histological examination of this specimen showed that there was cancer in the upper left side of the specimen (the cancer lesions are outlined in figure 4d by a blue marker) while the lower left and right side contained mostly normal adipose tissue. The middle section of this specimen contained mostly normal fibrous tissue. In the NIR autofluorescence images, the upper left side of the specimen exhibits higher intensity which is consistent with the presence of cancer in this side. However, the color image of the specimen may suggest, at least to the untrained eye, that the left side of this specimen in normal adipose tissue. In any case, the NIR autofluorescence image correctly highlighted the presence of cancer. One can also notice that the fibrous tissue in the NIR autofluorescence image obtained under 632.8-nm excitation has relatively lowered intensity to that observed in the corresponding image under 532-nm excitation. This effect that has been quantified in the analysis of our experiments by the lower ratio between cancer and fibrous tissue for 532-nm excitation compared to that under 632.8-nm excitation (see table 1).

Discussion

It has been hypothesized that emission by porphyrins present at different concentrations in tumor tissue compared to corresponding normal tissue gives rise to difference in the NIR emission intensity allowing visualization of the tumor by imaging [16]. Zhang et al demonstrated that this signal has a lifetime on the order of 1 ns, thus it is due to emission by a tissue chromophore [15] but, to the best of our knowledge, an exact identification has not yet been made. Increased porphyrin production has been observed in multiple cancer types including cancers as diverse as breast, colon, endocrine, kidney, liver or lymphomas [18-20] supporting the assignment of porhyrins as the responsible fluorophore. This work does not offer any additional information that could help resolve this issue. It is our intention to further investigate this issue by combining spectroscopic imaging measurements under variable excitation with analytical methods. This will reveal the excitation spectral regions where the contrast is maximized for a direct comparison with the absorption spectra of known tissue chromophores and their measured concentration within the imaged tissue components.

The NIR autofluorescence images from the tissue specimens were complemented with cross-polarized light scattering images in order to investigate for a possible systematic dependence of the autofluorescence intensity with the scattering properties of the tissue components. Cross-polarized imaging was preferred because it is based on photons that have interacted with the tissue to lose their polarization thus bearing information about the optical properties of the tissue components [21]. The experimental results shown in figures 3a, 3b and 3c and summarized in table 1 indicate that 532-nm excitation provides higher contrast than 632.8-nm excitation between cancer and adipose tissue. The mean value of the cancer/adipose intensity ratio is 2.62 under 532-nm excitation and 2.06 under 632.8 nm excitation. The difference observed in the light scattering images at 700-nm was much lower with a mean value of 1.21. On the other hand, 632.8 nm excitation offers higher contrast between tumor and

normal fibrous tissue. More specifically, the mean value of the cancer/fibrous intensity ratio is 1.34 under 532-nm excitation and 1.49 under 632.8 nm excitation. In at least one case the ratio under 532-nm excitation is close to 1 making visualization of the tumor from the surrounding normal fibrous tissue impossible. The corresponding mean value of the intensity ratio between tumor and normal fibrous tissue in the light scattering images was 1.09. In fact, only one of the specimens had a ratio between normal fibrous and tumor larger that 1.2 while half of the specimens had a ratio of ≈1 (see fig. 3b). This indicates that the origin of the differences in the NIR autofluorescence intensity is not the light scattering properties of the tissues but rather the concentration within the tissue of a fluorescing substance. This is in agreement with the previous report using specimens obtained from various body parts [16].

Another characteristic difference in the autofluorescecne intensiy observed under 532-nm and 632-nm excitation is revealed by the measured intensity ratio between fibrous and adipose tissue. The measured mean value of this ratio is 2.26 under 532-nm excitation compared to 1.30 under 632.8 nm excitation. The value of the fibrous/adipose ratio under 532 nm excitation is not very different to that obtained for the cancer/adipose ratio (2.62). This means that using 532 nm excitation it will be difficult to distinguish between normal fibrous and cancer tissue in a field of view that contains mostly adipose tissue. In contrast, 632.8-nm excitation provides a considerably larger contrast between cancer and adipose tissue compared to fibrous and adipose tissue as revealed by the corresponding intensity ratios of 2.06 and 1.30, respectively. These observations suggest that the red excitation provides a better imaging method for breast cancer detection. This property in combination with the fact that red light offers larger penetration depth while absorption by blood is reduced suggests an advantage in using excitation in the red spectral region. Arguably, the longer photoexcitation and imaging wavelengths used in this work that propagate deeper into tissue to probe a larger tissue volume and not only the surface, are more appealing. In addition, lesions that may be located below the

surface of the tissue (and thus being invisible to the naked eye) can cause enhancement of the image intensity offering the possibility for detection of subsurface tumors. Furtheremore, artifacts arising by blood are minimized due to the lower absorption coefficient of hemoglobin in the red spectrum. For in-vivo application of this method, the strong absorption by blood in the green spectrum may hinder its clinical applicability. On the other hand, the absorption coefficient in the red is smaller by about two orders of magnitude and consequently, small amounts of blood will not affect the images.

One of the specimens in this study (case 2) contained four cancer lesions having diameter of 1 mm or smaller. All lesions were located in a field of connective tissue and were clearly visible in the autofluorescence images under 632.8-nm excitation (see results for case 2 in figs. 3a, 3b and, 3c). However, these lesions were not visible under 532-nm excitation or with NIR light scattering. In addition, in three cases the tumor contained elongated extensions from the central mass that were about 1 mm in width. These lesions were also visible in the NIR autofluorescence images with the 632-nm excitation offering better visualization than 532-nm excitation. These experimental results indicate that detection of sub-millimeter in size lesions using NIR autofluorescence is feasible. This issue has also been discussed in more detail in ref. 16. The sensitivity in detecting small lesions is critical for in vivo use of this method for the examination of the margins. We plan to test the detection limits of this method by increasing the spatial resolution of the imaging system.

The error bars shown in the data displayed in figures 3a, 3b and, 3c vary considerably. This variation in the intensity ratios between the three main breast tissue components may be attributed in part to the depth of each lesion and the type of tissue located underneath the superficial lesion. Due to the long excitation and emission wavelength (especially under red excitation), the image may arise from autofluorescence from more than one tissue components

when the exposed on the surface lesion is thin. This phenomenon may be of importance for in vivo evaluation of the margins and we plan to father investigate its importance.

As more woman with early-stage breast cancer (DCIS or Stage I, IIA, IIB, or IIIA) are now presented with the choice of a breast-sparing surgery (surgery that removes the cancer and leaves most of the breast), it is essential to optimize the patient's quality of life and health after treatment. It is estimated that 40-70% of margins from breast lumpectomies will be involved by malignancy if the excision was not preceded by a tissue diagnosis. Similar to the above discussion, a margin involved by malignancy would require another surgical procedure. Our experimental results suggest that this method is able to detect invasive carcinoma and provide information in real time to help more accurately determine the status of the margins in vivo, while the patient is still in the operating room. Optical imaging could be most useful for the detection of nonpalpable or very small lesions and therefore guide the surgeon. Upon validation of this method, this information could be used intraoperatively to direct the need for additional surgery (i.e., axillary nodal staging, mastectomy, etc.).

We envision the utilization of this method in a clinical setting using an imaging system that captures NIR autofluorescence images of the tissue with an adjustable spatial resolution using excitation in the red spectrum from a laser or a diode light source. These images can then be used to detect and image cancer in real time. The experimental results suggest a large difference between cancer and adipose tissue (ratio of ≈2) and between cancer and fibrous tissue (ratio of ≈1.5). This system however may only to be used as a guidance tool for the surgeon but not for automated diagnosis for two main reasons. a) The intensity difference between fibrous and adipose tissue is about the same as that between cancer and fibrous tissue (≈1.3 vs ≈1.5). It is therefore necessary for an operator to visually inspect the tissue and make an assessment whether the lower in intensity component is fibrous (and therefore the higher in intensity features are possibly cancer) or adipose. It is possible however to incorporate

light scattering measurement in the visible spectrum for the separation of the fibrous (which is reddish in color) from the adipose tissue (yellowish in color). Furthermore, one could normalize an image to the signal intensity observed from fibrous tissue and then consider values larger than ≈ 1.3 X the normalized intensity as potentially cancerous lesions (see table 1). b) The breast tissue anatomy is more complex than that considered in this manuscript. It is therefore essential that the operator of such system be able to directly correlate the imaging information with the anatomical structure of the tissue. We plan to test this technique using a NIR autofluorescence imaging system under 632-nm excitation in ex-vivo large specimens obtained following lumpectomies or mastectomies for a more accurate assessment of the usefulness as well as the sensitivity and specificity of this method.

The results demonstrated by this method may also be very useful in the development of the Breast Cancer Optical Biopsy Needle, a design that has been proposed as a minimally invasive cancer detection and/or diagnosis tool for the breast [22]. This system uses fibers and other sensors to interrogate the optical as well as electrophysiological and structural properties of the tissue while the location of the tip of the needle is simultaneously recorded. The incorporation of the measurement of the NIR autofluorescence intensity under both, green and red excitation may be very useful in this system for more accurate detection of cancer and characterization of the tissue components.

Acknowledgements

This work was performed in part at UC, Lawrence Livermore National Laboratory under the auspices of the U.S. Department of Energy under Contract W-7405-Eng-48. This research is supported by funding from the California Breast Cancer Research Program and the National Science Foundation. The Center for Biophotonics, an NSF Science and Technology Center, is

managed by the University of California, Davis, under Cooperative Agreement No. PHY 0120999.

References

[1] AM Kavanagh, H Mitchell, GG Giles. “Hormone replacement therapy and accuracy of mammographic screening”, LANCET, **355** 1726, (2000).

[2] E. Lundstrom, B. Wilczek, Z. von Palffy, G. Soderqvist, B. von Schoultz, “Mammographic breast density during hormone replacement therapy differences according to treatment”, Am J Obstet Gynecol., **181**, 348, (1999).

[3] G.N. Hortobagyi, “Treatment of breast cancer”, N Engl. J Med., **339**, 974, (1998)

[4] M. A. Franceschini, K. T. Moesta, S. Fantini, G. Gaida, E. Gratton, H. Jess, W. W. Mantulin, M. Seeber, P. M. Schlag, M. Kaschke, “Frequency-domain techniques enhance optical mammography: Initial clinical results”, P Natl Acad Sci, **94**, 6468 (1997)

[5] S. B. Colak, M. b. van der Mark, G. W. Hooft, J. H. Hoogenraad, E. S. van der Linden, F. A. Kuijpers, “Clinical optical tomography and NIR spectroscopy for breast cancer detection”, IEEE J Sel Top Quant, **5**, 1143, (1999)

[6] V. Ntziachristos, B. Chance, “*Probing physiology and molecular function using optical imaging: applications to breast cancer”,* Breast Cancer Res, **3**, 41, (2001).

[7] T. Boehm, A. Hochmuth, A. Malich, J. R. Reichenbach, M. Fleck, W. A. Kaiser, “Contrast-enhanced near-infrared laser mammography with a prototype breast scanner - Feasibility study with tissue phantoms and preliminary results of imaging experimental tumors”, Investigative Radiology, **36**, 573, (2001).

[8] V. Quaresima, S. J. Matcher, M. Ferrari “Identification and quantification of intrinsic optical contrast for near-infrared mammography” Photochemistry & Photobiology, **67**, 4-14, (1998)

[9] R. R. Alfano and B. R. Masters, Biomedical Optical Biopsy, Classic Reprints on CD-ROM, Vol. 2, OSA, 2004.

[10] C. J. Frank, D. C. Redd, T. S. Gansler, R. L. McCreery, “Characterization of human breast specimens with Near-IR Raman spectroscopy”, Anal. Chem. **66**(3), 319-326 (1994)

[11] R. Manoharan, K. Shafer, L. Perelman, J. Wu, K. Chen, G. Deinum, M. Fitzmaurice, J. Myles, J. Crowe, R. Dasari, M. S. Feld, “ Raman spectroscopy and fluorescence photon migration for breast cancer diagnosis and imaging” Photochemistry & Photobiology, **67**, 15-22, 1998.

[12] A. S. Haka, K. E. Shafer-Peltier, M. Fitzmaurice, J. Crowe, R. R. Dasari, M.S. Feld, “Identifying microcalcifications in benign and malignant breast lesions by probing differences in their chemical composition using Raman spectroscopy”, Cancer Research, **62**, 5375-5380, (2002).

[13] S. G. Demos, H. Savage, Alexandra S. Heerdt, S. Schantz and R.R. Alfano, “Time Resolved Degree of Polarization for Human Breast Tissue”, Optics Communications, **124**, 439, (1996)

[14] D. W. Chicken, A. C. Lee, G. M. Briggs, M. R. S. Keshtgar, K. S. Johnson, D. D. O.Pickard, I. J. Bigio, S. G. Bown, “Optical biopsy: A novel intraoperative diagnostic tool to determine sentinel lymph node status instantly in breast cancer”, Breast Cancer Research & Treatment, **82**, S172-S174 1014, 2003.

[15] Gang Zhang, S. G. Demos, and R.R. Alfano, "Far-red and NIR spectral wing emission from tissues under 532-nm and 632-nm photo-excitation", Lasers in the Life Sciences, **9**, 1-16 (1999).

[16] S. G. Demos, R. Gandour-Edwards, R. Ramsamooj, R. deVere White, “Near infrared autofluorescence imaging for detection of cancer”, Journal of Biomedical Optics 9, 587–592, 2004

[17] S. G. Demos, R. Gandour-Edwards, R. Ramsamooj, R. deVere White, “Spectroscopic detection of bladder cancer using near infrared imaging techniques”,. Journal of Biomedical Optics **9**, 767-771, 2004

[18] M.M.H. El-Sharabasy, A.M. El-Wassel, M.M. Hafez and S.A. Salim, “Porphyrin metabolism in some malignant diseases”, Br. J. Cancer, 65, 409-412, (1992)

[19] L. Rasetti, G.F. Rubino, L. Tettinatti and G.W. Drago, “Porphyrin porphobilinogen and amino ketone levels in tumor tissue”, Panminerva Med. 7, 105-110, (1965)

[20] Zawirska, B., “*Comparative porphyrin content in tumors with contiguous non-neoplastic tissues”,* Neoplasma, 26, 223-9, 1979.

[21] S. G. Demos and R.R. Alfano, “Optical Polarization Imaging”, Applied Optics, **36**, 150-155, (1997).

[22] R. Andrews, R. Mah, L. Da Silva, “The NASA smart probe project for real-time multiple-microsensor tissue recognition” SPIE Proceedings, **5326**, 92-97, 2004 **.**

Figure and Table captions

Table 1: Mean values and standard deviation of the ratio of image intensities from cancer and normal (adipose and fibrous) tissues components as recorded in the NIR autofluorescence images under 532-nm and 632.8-nm excitation and in the cross-polarized light scattering images under 700-nm illumination

Figure 1: NIR autofluorescence image under a) 532 nm excitation and b) 632,8 nm excitation of a 4-cm X 3-cm human breast tissue, ≈6-mm thick. c) A contrast-enhanced H&E stained paraffin section of the same specimen with tumor location indicated by an arrow. d) Intensity profiles of images (a) and (b) along a vertical line passing through the middle of the tumor.

Figure 2: NIR autofluorescence images of a ≈ 2.8x4 cm^2 section of breast tissue under a) 532 nm and b) 632,8 nm excitation. C) H&E stained paraffin section of the same specimen.

Figure 3: The ratio of the intensities from human breast tissue components obtained from the NIR autofluorescence images under 532-nm and 632.8-nm excitation and from the cross-polarized light scattering images under 700-nm illumination. Intensity ratio between a) tumor and normal adipose, b) tumor and fibrous and c) fibrous and adipose tissues.

Figure 4: The NIR autofluorescence images of a ≈ 3.2x4.2 cm^2 specimen under a) 532 nm and b) 632,8 nm excitation. c) A color photograph of the same specimen. d) A contrast-enhanced H&E stained paraffin section of the same specimen with tumor regions outlined with blue marker.

Table 1

	Mean value / Standard Deviation		
	532-nm excitation	632.8-nm excitation	700-nm illumination
CA/Adipose	**2.62** / 0.67	**2.06** / 0.55	**1.21** / 0.17
Cancer/Fibrous	**1.34** / 0.11	**1.49** / 0.27	**1.09** / 0.14
Fibrs /Adipose	**2.26** / 0.52	**1.30** / 0.12	**1.12** / 0.20

Figure 1

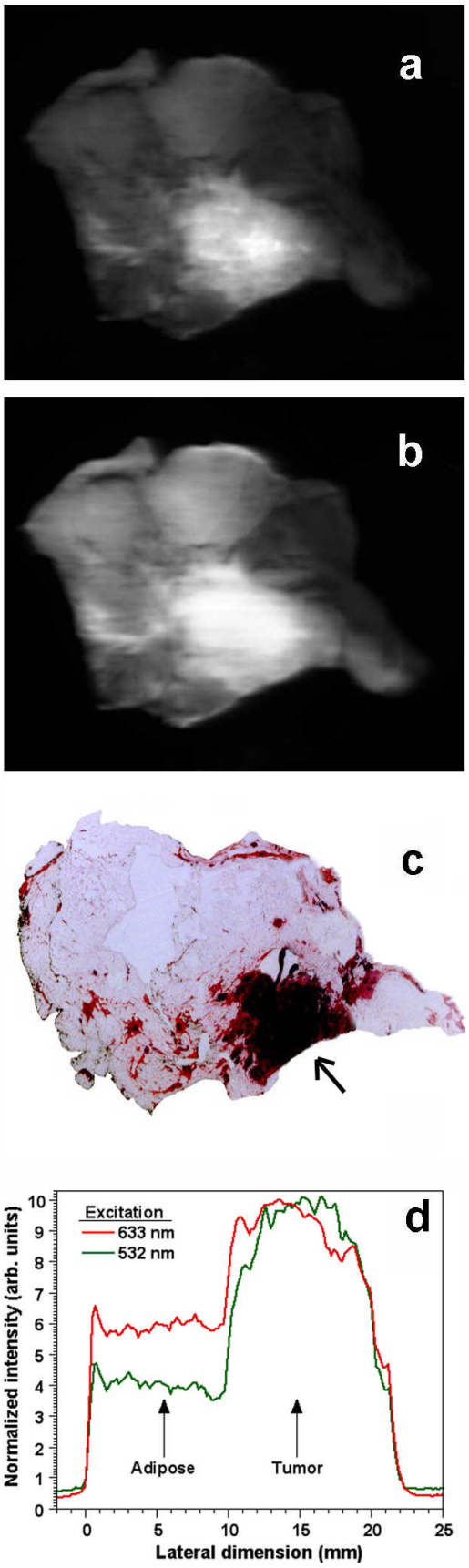
a
b
c
d
Excitation
633 nm
532 nm
Normalized intensity (arb. units)
Adipose
Tumor
Lateral dimension (mm)
0
1
2
3
4
5
6
7
8
9
10
0
5
10
15
20
25

Figure 2

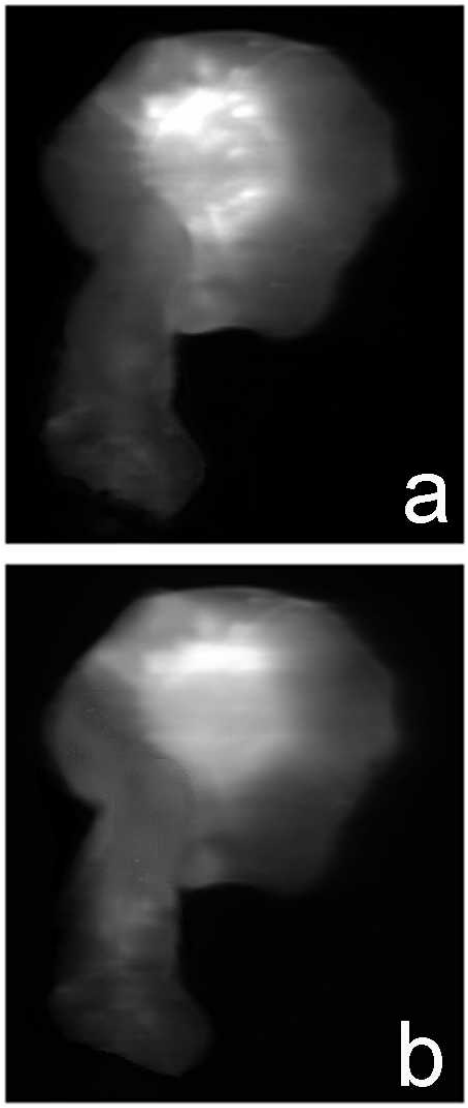

Figure 3a

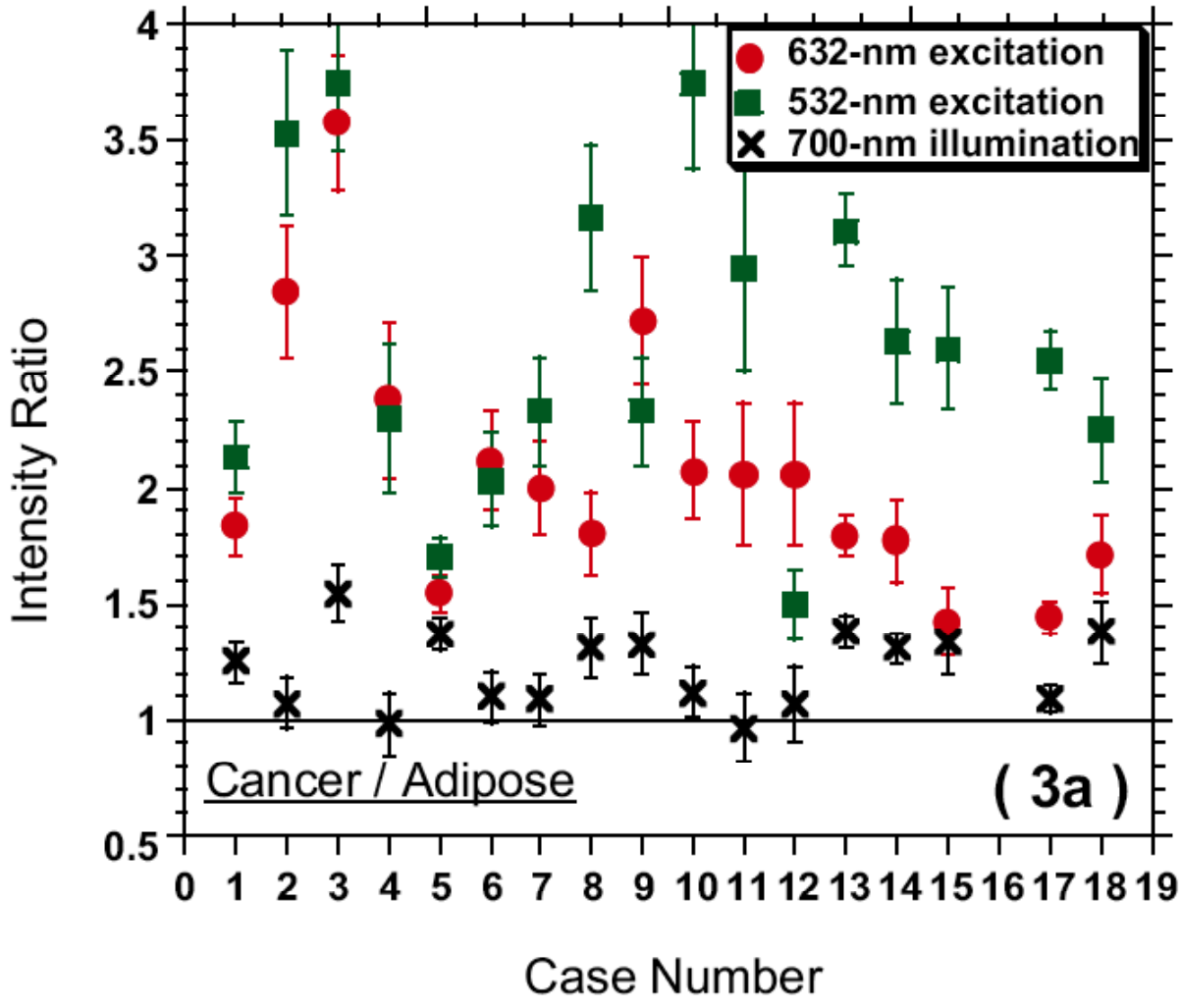
632-nm excitation
532-nm excitation
700-nm illumination
Intensity Ratio
Case Number
Cancer / Adipose
(3a)
0.5
1
1.5
2
2.5
3
3.5
4
0 1 2 3 4 5 6 7 8 9 10 11 12 13 14 15 16 17 18 19

Figure 3b

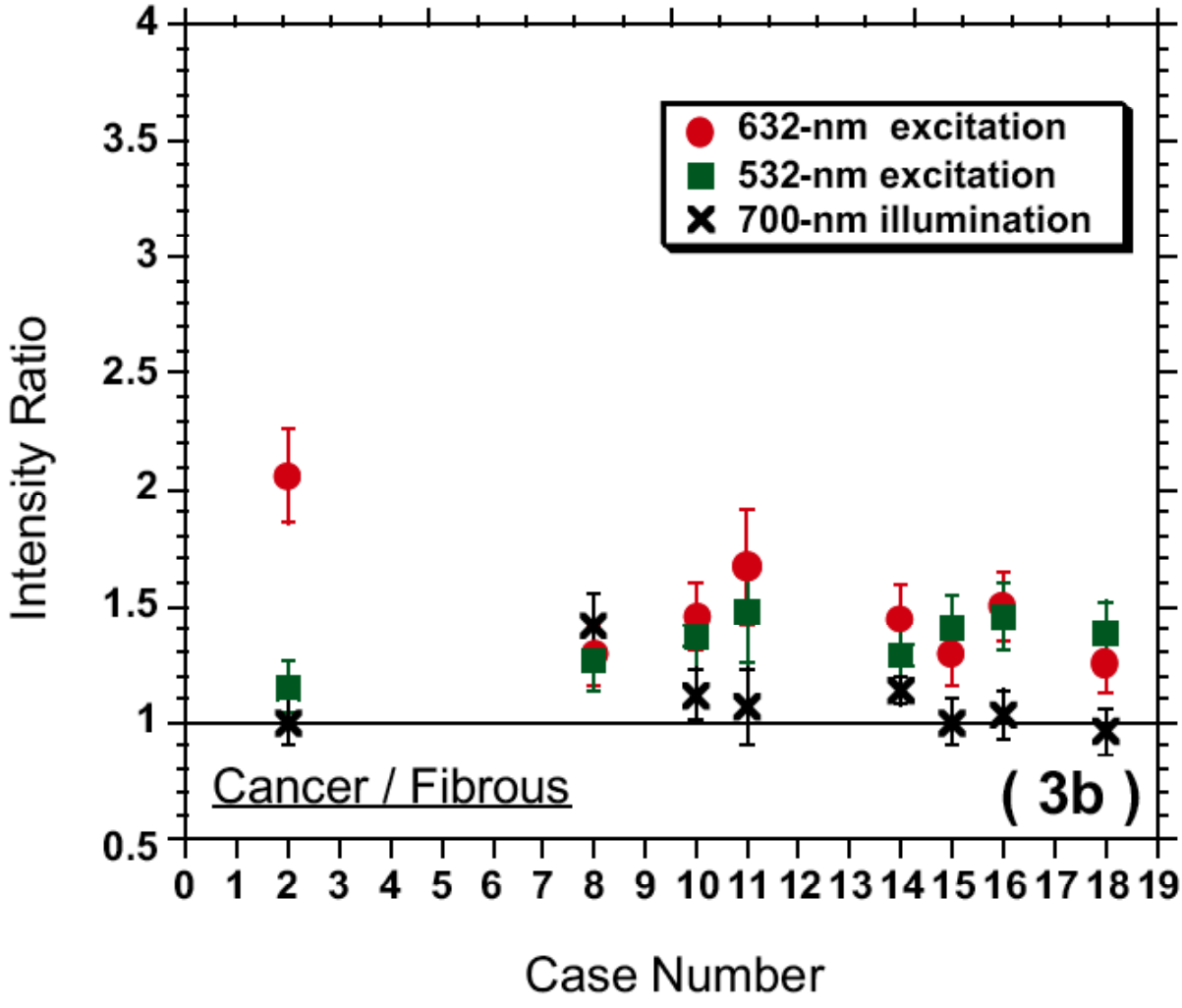
632-nm excitation
532-nm excitation
700-nm illumination
Intensity Ratio
Case Number
Cancer / Fibrous
(3b)
4
3.5
3
2.5
2
1.5
1
0.5
0 1 2 3 4 5 6 7 8 9 10 11 12 13 14 15 16 17 18 19

Figure 3c

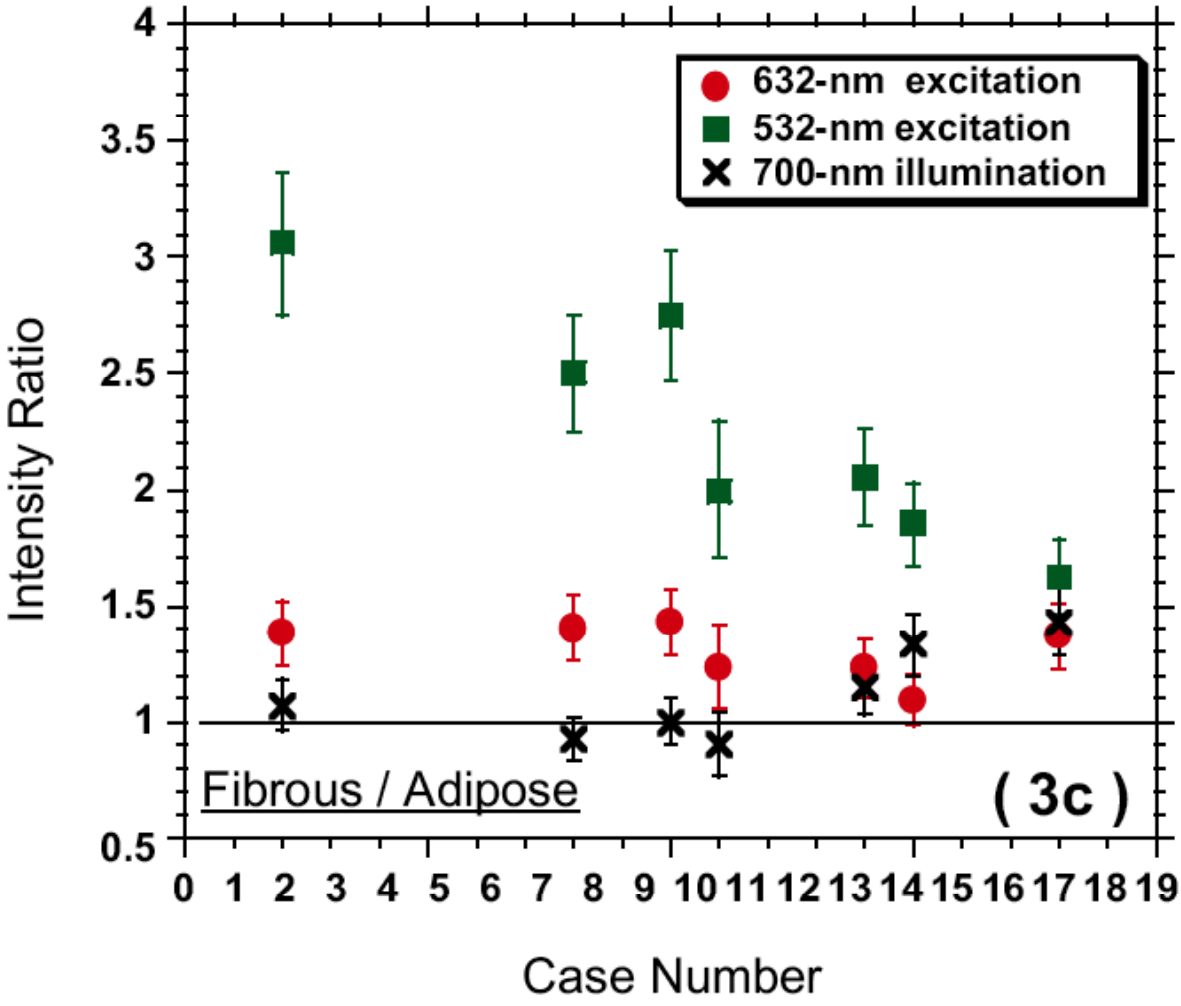
632-nm excitation
532-nm excitation
700-nm illumination
Intensity Ratio
Case Number
Fibrous / Adipose
(3c)
4
3.5
3
2.5
2
1.5
1
0.5
0 1 2 3 4 5 6 7 8 9 10 11 12 13 14 15 16 17 18 19

Figure 4